GENERALIZED MOMENTUM CONTROL OF THE SPIN-STABILIZED MAGNETOSPHERIC MULTISCALE FORMATION

Steven Z. Queen,[*] **Neerav Shah**,[*] **Suyog S. Benegalrao**,[*] **and Kathie Blackman**[†]

The Magnetospheric Multiscale (MMS) mission consists of four identically instrumented, spin-stabilized observatories elliptically orbiting the Earth in a tetrahedron formation. The on-board attitude control system adjusts the angular momentum of the system using a generalized thruster-actuated control system that simultaneously manages precession, nutation and spin. Originally developed using Lyapunov control-theory with rate-feedback, a published algorithm has been augmented to provide a balanced attitude/rate response using a single weighting parameter. This approach overcomes an orientation sign-ambiguity in the existing formulation, and also allows for a smoothly tuned-response applicable to both a compact/agile spacecraft, as well as one with large articulating appendages.

INTRODUCTION

The Magnetospheric Multiscale (MMS) mission, launched on March 13, 2015, is the fourth mission of NASA's Solar Terrestrial Probe program. The MMS mission consists of four identically instrumented observatories that function as a constellation to provide the first definitive study of magnetic reconnection in space.

Since it is frequently desirable to isolate electric and magnetic field sensors from stray effects caused by the spacecraft's core-body, the suite of instruments on MMS includes six radial and two axial instrument-booms with deployed lengths ranging from 5–60 meters (see Figure 1). The observatory is spin-stabilized about its positive z-axis with a nominal rate slightly above 3 rev/min (RPM). The spin is also used to maintain tension in the four radial wire booms.

Both attitude and orbital control of the observatories are accomplished using twelve hydrazine mono-propellant thrusters—four AMPAC 1-lbf (4.4 N) thrusters are directed axially (±z), and eight Aerojet 4-lbf (17.8 N) thrusters radially (±y). The minimum impulse bit for the Aerojet designed thrusters ranges throughout the mission from 0.13–0.26 N-m-sec, which corresponds to a 20 millisecond pulse.

An assortment of attitude control requirements were levied upon the system. Each of these criteria are to be achieved for a fully-deployed observatory configuration. These requirements include the capability to orient the spacecraft's spin-axis 10-degrees from the ecliptic normal, modify observatory spin rate to within 0.2 RPM of the commanded level, adjust the observatory orientation

---

[*] Aerospace Engineer, Attitude Control Systems Engineering Branch, NASA/GSFC, Greenbelt, MD.
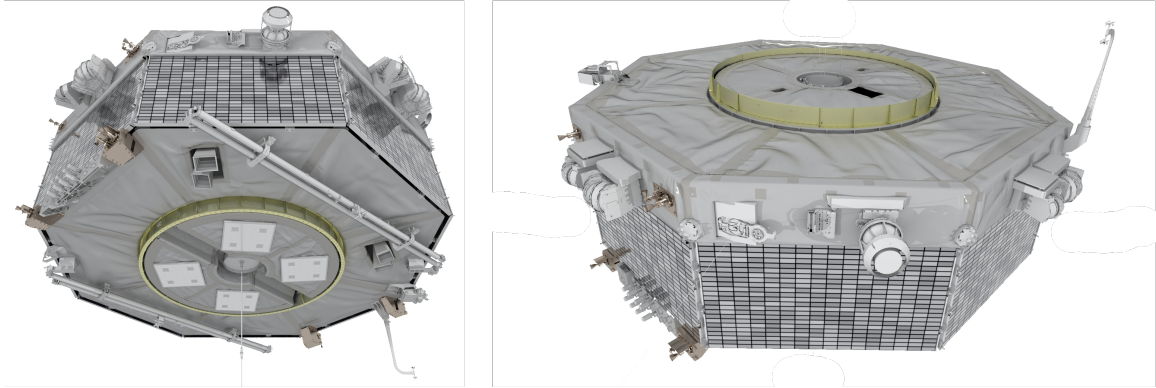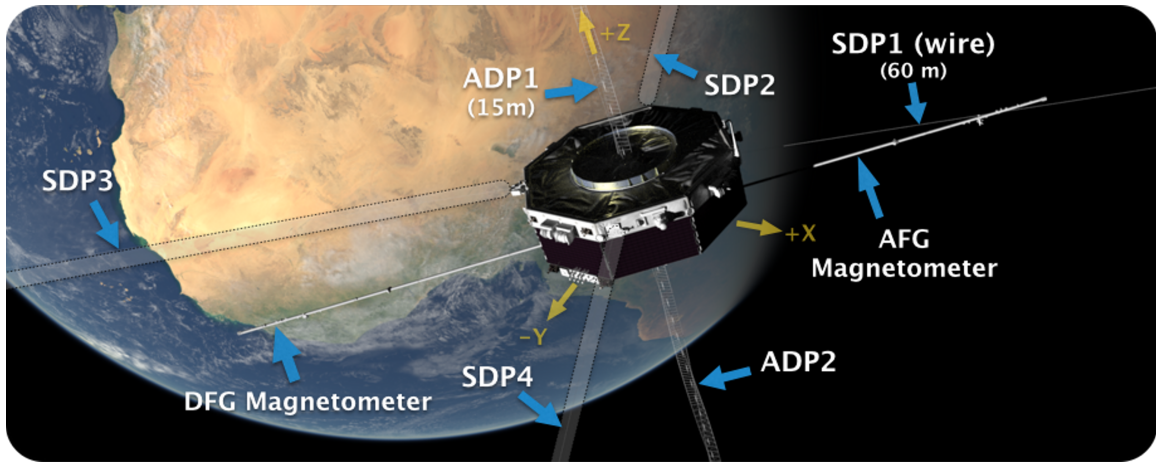[†] Aerospace Engineer, the Hammers Company, Greenbelt, MD.

Figure 1. MMS Observatory Fully-Deployed (top) and Stowed (bottom)

to maintain optimal science-data gathering in the presence of gravity gradient disturbances and solar aspect angle motion, and perform these maneuvers so as to minimize wire boom in-plane and out-of-plane deflection angles.

Attitude and rate determination for MMS is achieved by using a Multiplicative Extended Kalman Filter[1, 2] to process the quaternion measurements produced by the μASC Star Tracker System (STS), provided by the Technical University of Denmark (DTU). The STS consists of internally redundant electronics, housed within a single enclosure, that interfaces with four Charge-Coupled Device camera head units. The STS provides time-stamped attitude quaternion data packets at a 4 Hz telemetry rate. It has a 3σ performance transverse and bore-sight axis accuracy of 60 arcsec and 200 arcsec, respectively. The STS has a spin rate capability of up to 4 RPM, and has demonstrated limited functionality up to 5 RPM.

MMS is also equipped with an Adcole digital sun-sensor for use in contingencies, and by the science suite as a time-reference.

One possible scheme for controlling a spacecraft's spin-dynamics is to use decoupled momentum adjustment maneuvers. Full system control would be achieved via a combination of sequential precession maneuvers, spin-rate adjustments, and active/passive nutation damping.[3] There were two atypical aspects of the MMS mission that made this traditional approach an unattractive design choice—the long flexible wire booms, and the operational cadence of managing a formation of

four spacecraft in real-time with limited communication-network and staffing resources. With the four symmetric Spin-plane Double Probe (SDP) wire booms extending 60-meters radially from the central bus, timing open-loop thruster pulses to accurately adjust the momentum of the system proved to be a non-trivial task. Furthermore, the prospect of iterating between precession, spin and nutation adjustments did not seem tractable given both the frequency of planned maneuvers and the complex gyrodynamic cross-coupling after all appendages are deployed.

For all of the above reasons, a unified closed-loop momentum-management design was sought that would simultaneously control all the aspects of spin-stabilization without the need for iterative maneuvering, extended settling-times, or dedicated damping hardware. Ultimately, the complete solution for MMS was found by expanding upon the framework originally developed by Reynolds and Creamer for the Reuven Ramaty High Energy Solar Spectroscopic Imager (RHESSI) mission.[4] Flight results from the MMS fleet's commissioning maneuvers have proven the final Delta-H Mode controller design to be both accurate and operationally simple. Furthermore, with only a minimal number of parameter changes, the same controller performed well for both the all-stowed and fully-deployed observatory configurations.

LYAPUNOV CONTROL

Lyapunov's direct method provides a tool for making analytical stability claims of nonlinear systems (such as a tri-axial spinning spacecraft) with the major benefit of not having to explicitly solve the nonlinear differential equations. Simply paraphrased, if a Lyapunov function $V(\mathbf{x})$ exists for a (nonlinear) dynamical system $\dot{\mathbf{x}} = f(\mathbf{x})$, then the system is stable about an (equilibrium) point. A scalar function, $V(\mathbf{x})$, qualifies as a Lyapunov function for the dynamical system if it is continuous and there exists a neighborhood about the equilibrium point such that for any $\mathbf{x}$,

1. $V(\mathbf{x})$ is a positive definite function about the origin
2. $V(\mathbf{x})$ has a continuous partial derivative
3. $\dot{V}(\mathbf{x})$ is negative semi-definite

Note that while the Lyapunov function explicitly depends only on the state-vector $\mathbf{x}$, $V(\mathbf{x})$ is time-varying because $\mathbf{x}(t)$ is itself time-varying.[5]

If the expression of the system dynamics, $\dot{\mathbf{x}} = f(\mathbf{x})$, includes closed-loop control inputs $\mathbf{u}(t)$, then the Lyapunov direct method also becomes a tool for control law design. Specifically, the control input $\mathbf{u}$ is applied in such a manner that the first derivative of the selected Lyapunov function, $\dot{V}(\mathbf{x})$, remains negative semidefinite and the applied control is stabilizing, i.e. drives the system towards our desired reference state (or trajectory).

A common barrier in applying Lyapunov's direct method is frequently the selection of a "good" Lyapunov function. This is the only part of the analysis that requires some intuition about the desired behavior of the system—the remainder of the control-design procedure is quite systematic. In order to alleviate some of the murkiness surrounding function selection, the following subsections examine a family of Lyapunov functions and their practical implications for control of spinning spacecraft.

Rate Control (Spin and Nutation)

In the case of a rigid-body spacecraft equipped with actuators capable of introducing a control-torque $\boldsymbol{\tau}(u)$, the appropriate system dynamics (i.e. $\dot{\mathbf{x}} = f(\mathbf{x}, \mathbf{u})$) are *Euler's rotational equation*

expressed as matrices (bold upper-case symbols) and column vectors (lower-case bold symbols)

$$\tau = \dot{\mathbf{h}} + [\boldsymbol{\omega}]^\times \mathbf{h} \tag{1}$$

$$= \mathbf{I}\dot{\boldsymbol{\omega}} + [\boldsymbol{\omega}]^\times \mathbf{I}\boldsymbol{\omega} \tag{2}$$

$$\dot{\boldsymbol{\omega}} = \mathbf{I}^{-1}\left(\tau - \boldsymbol{\omega}^\times \mathbf{I}\boldsymbol{\omega}\right) \tag{3}$$

where $\mathbf{h}$ is the body's angular momentum about its center-of-mass, $\boldsymbol{\omega}$ is the angular rate of the body (and body-fixed frame) with respect to an inertial reference, $\mathbf{I}$ is the second mass-moment of inertia matrix about the center-of-mass, an over-dot $(\dot{})$ indicates the time-derivative with respect to the body-frame, and the superscript expression $[]^\times$ indicates a skew-symmetric 3×3 matrix formed from its base vector. All quantities are expressed in a body-fixed frame whose origin is at the center-of-mass.

$$\boldsymbol{\omega}^\times = \begin{bmatrix} \omega_x \\ \omega_y \\ \omega_z \end{bmatrix}^\times = \begin{bmatrix} 0 & -\omega_z & \omega_y \\ \omega_z & 0 & -\omega_x \\ -\omega_y & \omega_x & 0 \end{bmatrix} \tag{4}$$

With mechanical systems, a good place to start when considering Lyapunov function candidates is the system's kinetic energy. It has the desired property of being both a scalar and quadratic in rate (i.e. positive definite). The Lyapunov function V_1 equal to the rotational kinetic energy $\mathsf{E_k}$ of a rigid body is,

$$V_1 = \mathsf{E_k} = \frac{1}{2}\boldsymbol{\omega}^\mathsf{T}\mathbf{I}\boldsymbol{\omega} \tag{5}$$

$$= \frac{1}{2}\mathbf{h}^\mathsf{T}\mathbf{I}^{-1}\mathbf{h} \tag{6}$$

where the superscript $^\mathsf{T}$ denotes a matrix transpose. Taking the total time-derivative of Lyapunov function V_1 yields

$$\dot{V}_1 = \frac{d}{dt}V_1 = \frac{\partial V}{\partial \mathbf{x}}\dot{\mathbf{x}} = \frac{\partial V}{\partial \mathbf{x}}\mathbf{f}(\mathbf{x}) \tag{7}$$

$$= \frac{1}{2} \cdot \frac{d}{dt}\left(\boldsymbol{\omega}^\mathsf{T}\mathbf{I}\boldsymbol{\omega}\right) \tag{8}$$

$$= \boldsymbol{\omega}^\mathsf{T}\mathbf{I}\dot{\boldsymbol{\omega}} \tag{9}$$

$$= \boldsymbol{\omega}^\mathsf{T}\left(\tau - \boldsymbol{\omega}^\times \mathbf{I}\boldsymbol{\omega}\right) \tag{10}$$

$$= \boldsymbol{\omega}^\mathsf{T}\tau \tag{11}$$

Enforcing Lyapunov stability requires that $\dot{V}_1 \leq 0$ and that implies the dot-product $\boldsymbol{\omega}^\mathsf{T}\tau$ is also negative semi-definite—in other words the control-torque $\tau(u)$ must always be opposite the direction of the rate (or zero). Two details of the mathematics are worth noting. First, the scalar triple-product relationship was used, which states that if any two vectors in the product $\mathbf{a}^\mathsf{T}[\mathbf{b}]^\times \mathbf{c}$ are equal (e.g. $a = b$, $a = c$, etc.) then the entire product is zero. Second, taking the time-derivative of the scalar function V_1 consisting of quantities expressed in the body-frame involves taking *local* derivatives of $\boldsymbol{\omega}$ and $\mathbf{I}$ with respect to the body-frame (e.g. $\mathbf{I}$ is constant).

While function V_1 produced a trivial result—a pure rate damper—a more useful control law may be obtained by moving the reference point for the velocity state away from the origin. This is done

through a change of variables

$$\boldsymbol{\delta h} = \mathbf{h} - \mathbf{h}_{\text{ref}} \qquad (12)$$

where we select $\mathbf{h}_{\text{ref}}$ to be a desired target for the angular momentum expressed in the body-frame. Applying the change of variables to Eq. (6) results in new candidate function, V_2, as follows

$$V_2 = \frac{1}{2}\boldsymbol{\delta h}^{\mathsf{T}}\mathbf{I}^{-1}\boldsymbol{\delta h} \qquad (13)$$

With first-derivative

$$\dot{V}_2 = \boldsymbol{\delta h}^{\mathsf{T}}\mathbf{I}^{-1}\boldsymbol{\delta \dot{h}} \qquad (14)$$

$$= \boldsymbol{\delta h}^{\mathsf{T}}\mathbf{I}^{-1}\left(\dot{\mathbf{h}} - \dot{\mathbf{h}}_{\text{ref}}\right) \qquad (15)$$

If the momentum reference target is chosen to be equivalent to a constant magnitude spin ω_0 about the major principal axis unit-direction $\hat{\mathbf{p}}_3$ (where $I_3 > I_2 \geq I_1$), then $\dot{\mathbf{h}}_{\text{ref}} = \mathbf{0}$ and Eq. (15) takes the form

$$\dot{V}_2 = \boldsymbol{\delta h}^{\mathsf{T}}\mathbf{I}^{-1}\left(\boldsymbol{\tau} - \boldsymbol{\omega}^{\times}\mathbf{h}\right) \qquad (16)$$

$$= \left(\boldsymbol{\omega} - \boldsymbol{\omega}_{\text{ref}}\right)^{\mathsf{T}}\boldsymbol{\tau} + \boldsymbol{\omega}_{\text{ref}}^{\mathsf{T}}\boldsymbol{\omega}^{\times}\mathbf{I}\boldsymbol{\omega} \qquad (17)$$

where $\boldsymbol{\omega}_{\text{ref}} = \omega_0\hat{\mathbf{p}}_3$. Here the negative semi-definite requirement $\dot{V}_2 \leq 0$ for stability indicates that the control-torque should only be applied when it is aligned opposite the direction of the rate-error *and* exceeds a certain threshold. The result is combined spin and nutation control.

This is simple logic to implement in a digital controller, given a body-fixed actuator such as a thruster. If instead of a thruster, the designer has more freedom regarding the direction of the applied torque, then more analysis is required to determined the optimal direction to apply the control. That problem, along with other efficiency concerns, will be discussed in later sections.

By now the methodology for constructing Lyapunov-based controllers has emerged—define a quadratic cost function in terms of the states, take its derivative, substitute in the system dynamics, and finally construct a control-law constraining the derivative to be negative semi-definite. With this in mind, we explore two other Lyapunov functions that were used on flight systems and their performance implications.

Reynolds and Creamer Method (Spin, Nutation, and Pointing)

Until this point, all Lyapunov functions presented have been based purely on the rotational kinetic-energy of the system—solely functions of angular velocity. Like any traditional rate-only controller, no consideration is given to any of the positional-states. For the RHESSI mission, Reynolds and Cramer[4] developed a Lyapunov function that included a term quadratic in the angular momentum pointing-error linearly combined with a modified energy term. Their result has been recast in the present notation below

$$V_{\text{rc}} = \underbrace{\frac{1}{2}\left(\mathbf{h} - \mathbf{h}_{\text{pt}}\right)^{\mathsf{T}}\left(\mathbf{h} - \mathbf{h}_{\text{pt}}\right)}_{\text{pointing error}} + \underbrace{\left[\frac{1}{2}\mathbf{h}^{\mathsf{T}}\mathbf{I}^{-1}\mathbf{h} - \frac{1}{2}\mathbf{h}^{\mathsf{T}}\left(I_3\mathbb{1}\right)^{-1}\mathbf{h}\right]}_{\text{spin-rate "energy" error}} \qquad (18)$$

$$= \frac{1}{2}\left(\mathbf{h} - \mathbf{h}_{\text{pt}}\right)^{\mathsf{T}}\left(\mathbf{h} - \mathbf{h}_{\text{pt}}\right) + \frac{1}{2}\mathbf{h}^{\mathsf{T}}\left(I_3\mathbf{I}^{-1} - \mathbb{1}\right)\mathbf{h} \qquad (19)$$

5

where I_3 is the largest principal moment of inertia (i.e. maximum eigenvalue of $\mathbf{I}$), $\mathbb{1}$ is the 3×3 identity matrix, and $\mathbf{h}_{\mathsf{pt}}$ is the desired pointing momentum expressed in the body-frame. The angular momentum pointing-reference can be further expanded as

$$\mathbf{h}_{\mathsf{pt}} = H_0 \underset{b \leftarrow i}{\mathcal{A}} \hat{\mathbf{s}}_i \tag{20}$$

$$= I_3 \omega_0 \underset{b \leftarrow i}{\mathcal{A}} \hat{\mathbf{s}}_i \tag{21}$$

where H_0 $[\omega_0]$ is a constant representing the desired angular momentum [rate] magnitude, $\hat{\mathbf{s}}_i$ is unit-vector expressed in the inertial-frame that represents a desired pointing direction (fixed) in inertial space, and the symbol $\mathcal{A}$ we use generally to denote an attitude direction cosine matrix that, in this instance, transforms a vector from the inertial to body-fixed frame.

Differentiating the Reynolds-Creamer Lyapunov function produces

$$\dot{V}_{\mathsf{rc}} = (\mathbf{h} - \mathbf{h}_{\mathsf{pt}})^{\mathsf{T}} \left[\dot{\mathbf{h}} - \dot{\mathbf{h}}_{\mathsf{pt}} \right] + \mathbf{h}^{\mathsf{T}} \left(I_3 \mathbf{I}^{-1} - \mathbb{1} \right) \dot{\mathbf{h}} \tag{22}$$

$$= (\mathbf{h} - \mathbf{h}_{\mathsf{pt}})^{\mathsf{T}} \left[\boldsymbol{\tau} - \boldsymbol{\omega}^{\times} \mathbf{h} - H_0 (\underset{b \leftarrow i}{\dot{\mathcal{A}}} \hat{\mathbf{s}}_i + \underset{b \leftarrow i}{\mathcal{A}} \dot{\hat{\mathbf{s}}}_i) \right] + \mathbf{h}^{\mathsf{T}} \left(I_3 \mathbf{I}^{-1} - \mathbb{1} \right) \left(\boldsymbol{\tau} - \boldsymbol{\omega}^{\times} \mathbf{h} \right) \tag{23}$$

$$= (\mathbf{h} - \mathbf{h}_{\mathsf{pt}})^{\mathsf{T}} \left[\boldsymbol{\tau} - \boldsymbol{\omega}^{\times} (\mathbf{h} - \mathbf{h}_{\mathsf{pt}}) \right] + \mathbf{h}^{\mathsf{T}} \left(I_3 \mathbf{I}^{-1} - \mathbb{1} \right) \left(\boldsymbol{\tau} - \boldsymbol{\omega}^{\times} \mathbf{h} \right) \tag{24}$$

$$= (\mathbf{h} - \mathbf{h}_{\mathsf{pt}})^{\mathsf{T}} \boldsymbol{\tau} + \mathbf{h}^{\mathsf{T}} \left(I_3 \mathbf{I}^{-1} - \mathbb{1} \right) \boldsymbol{\tau} \tag{25}$$

$$= I_3 \left(\boldsymbol{\omega} - \omega_0 \underset{b \leftarrow i}{\mathcal{A}} \hat{\mathbf{s}}_i \right)^{\mathsf{T}} \boldsymbol{\tau} \tag{26}$$

$$= I_3 \cdot \boldsymbol{\delta\omega}_{\mathsf{rc}}^{\mathsf{T}} \boldsymbol{\tau} \tag{27}$$

Here again, liberal use was made of the scalar triple product identities to eliminate terms. The properties of an inertial-fixed target ($\dot{\hat{\mathbf{s}}}_i = 0$), as well as the definition of the attitude matrix derivative ($\dot{\mathcal{A}} = -\mathcal{A}\boldsymbol{\omega}^{\times}$) were also used in order to obtain the final expression. Finally, a new symbol for the rate-error ($\boldsymbol{\delta\omega}_{\mathsf{rc}} \equiv \boldsymbol{\omega} - \omega_0 \underset{b \leftarrow i}{\mathcal{A}} \hat{\mathbf{s}}_i$) was introduced.

The control law based on V_{rc} states that thrusters—or in the case of RHESSI, magnetic torque-rods—should only apply a moment to the spacecraft if the torque is aligned in the direction of the negative rate error. This guarantees convergence to a major-axis spin of the desired magnitude, and also pointing of the spacecraft angular momentum in the proper orientation in inertial space. In many ways, this is the complete solution for spinning spacecraft—simultaneous spin, nutation, and precession control with computationally simple logic.

Comparison to Quaternion-Feedback Control

For additional context, compare the Reynolds-Creamer control-law to the more widely known *quaternion-feedback*[6] control used to reorient (slew) three-axis stabilized spacecraft. The stability of the method was first demonstrated by Wie and Barba[7] using Lyapunov's direct method and a Lyapunov function equivalent to

$$V_{\mathsf{qf}} = \frac{1}{2} \boldsymbol{\omega} \mathbf{I} \boldsymbol{\omega} + \frac{1}{2} k_p \boldsymbol{\delta}\mathbf{q}_{1:3}^{\mathsf{T}} \boldsymbol{\delta}\mathbf{q}_{1:3} + \frac{1}{2} k_p (1 - \delta q_4)^2 \geq 0 \tag{28}$$

where $\boldsymbol{\delta}\mathbf{q}_{1:3}$ and q_4 are, respectively, the vector and scalar components of the attitude error quaternion ($\boldsymbol{\delta}\mathbf{q} \equiv \mathbf{q} \otimes \mathbf{q}_{\mathsf{ref}}^{-1}$), and k_p is a positive scalar gain.[1] This method achieves a final (inertial) reference attitude and nullifies the angular rate. The Reynolds-Creamer control-law achieves a result

similar to quaternion-feedback, but allows for a non-zero final rate and justifiably ignores clocking about the target (because of spin). One of the intended goals of this work is to raise the profile of Reynold's and Creamer's wonderfully intuitive and practical result. The present authors have become convinced this spin-stabilization technique should be a staple in every control engineer's toolbox.

Path Weighted Control (Nutation-Limiting, Spin-Preserving)

After adopting the Reynolds-Creamer control-law for MMS momentum management, and integrating its logic into a high-fidelity time-domain simulation of the system dynamics, a number of large-slew test-cases exposed an undesirable behavior of the controller. As similarly noted in the original development of quaternion-feedback,[7] the path taken by the system is not constrained by the control-logic. In the case of MMS, concerns were less focused on slew-path optimality, but instead on a more practical detriment—the rate could be driven through (or arbitrarily close) to zero-spin. This can be seen directly in the rate-error term of Eq. (26)—if $\boldsymbol{\omega}$ and $\hat{\mathbf{s}}_i$ are diametrically opposed, the torque that makes $\dot{V}_{\mathrm{rc}}$ negative semi-definite is opposite the current spin-vector.

Because of the need to maintain SDP wire boom tension (for the fully-deployed observatory), minimize transverse rates for the DTU star sensors, and preserve spin-polarity for the Adcole digital sun-sensors, arbitrary angular rates were an unacceptable artifact for the MMS design. In order to mitigate the problem, the Reynolds-Creamer Lyapunov function is augmented with a third term whose purpose is to limit nutation. This is implemented with an associated gain k_{spin} that allows for a continuous "mixing" of this new constraint with the existing pointing-error term. Linearly combining several elemental Lyapunov functions is a common technique.[5] The new *path weighted* control-Lyapunov function used on MMS becomes

$$V_{\mathsf{pw}} = \tfrac{k_{\mathsf{spin}}}{2}\left(\mathbf{h} - \mathbf{h}_{\mathsf{pt}}\right)^{\mathsf{T}}\left(\mathbf{h} - \mathbf{h}_{\mathsf{pt}}\right) + \tfrac{1-k_{\mathsf{spin}}}{2}\left(\mathbf{h} - \mathbf{h}_{\mathsf{b}}\right)^{\mathsf{T}}\left(\mathbf{h} - \mathbf{h}_{\mathsf{b}}\right) + \tfrac{1}{2}\mathbf{h}^{\mathsf{T}}\left(I_3\mathbf{I}^{-1} - \mathbb{1}\right)\mathbf{h} \quad (29)$$

$$= \underbrace{\tfrac{k_{\mathsf{spin}}}{2}\cdot\boldsymbol{\delta}\mathbf{h}_{\mathsf{pt}}^{\mathsf{T}}\boldsymbol{\delta}\mathbf{h}_{\mathsf{pt}}}_{\text{pointing error term}} + \underbrace{\tfrac{1-k_{\mathsf{spin}}}{2}\cdot\boldsymbol{\delta}\mathbf{h}_{\mathsf{b}}^{\mathsf{T}}\boldsymbol{\delta}\mathbf{h}_{\mathsf{b}}}_{\text{nutation term}} + \underbrace{\tfrac{1}{2}\mathbf{h}^{\mathsf{T}}\left(I_3\mathbf{I}^{-1} - \mathbb{1}\right)\mathbf{h}}_{\text{spin-rate ``energy'' error}} \quad (30)$$

In addition to the *ad hoc* angular velocity (kinetic-energy) term of the Reynolds-Creamer formulation, this new Lyapunov function contains two "potential-energy" terms—one constraining direction against an inertial target (pointing error term) and one against a body-fixed target (nutation term).

When the body-fixed angular momentum target is taken to be in the direction of the major principal axis ($\hat{\mathbf{p}}_3$), so that $\mathbf{h}_b = \omega_0\hat{\mathbf{p}}_3$, the system momentum is "encouraged" to remain in a region near a major-axis spin. This by definition limits nutation—the divergence of the angular momentum from a body's principal axis. The degree to which it is allowed to nutate is controlled by the mixing gain k_{spin}. This weighting is a necessary feature, because some nutation must be introduced into the system in order to reorient inertially. Furthermore, while the third term in Eq. (30)—the kinetic energy error—does by itself guarantee convergence to a major-axis spin, it does not discriminate on the final polarity. This is due to the fact that the energy is quadratic in angular velocity. Adding the additional nutation/potential term resolves this ambiguity.

Following a very similar derivation as the previous case, the associated time-derivative of the new Lyapunov function takes the form

$$\dot{V}_{\mathsf{pw}} = I_3 \left[\boldsymbol{\omega} - \omega_0 \left(k_{\mathsf{spin}} \underset{b \leftarrow i}{\mathcal{A}} \, \hat{\mathbf{s}}_i + (1 - k_{\mathsf{spin}}) \, \hat{\mathbf{p}}_3 \right) \right]^{\mathsf{T}} \boldsymbol{\tau} \tag{31}$$

$$= I_3 \, \delta\boldsymbol{\omega}_{\mathsf{pw}}^{\mathsf{T}} \, \boldsymbol{\tau} \tag{32}$$

and the logic necessary to ensure $\dot{V}_{\mathsf{pw}}$ is negative semi-definite is that the control-torque should only be applied in a direction opposite this new mixed angular rate error-"cocktail", $\delta\boldsymbol{\omega}_{\mathsf{pw}}$.

In Figure 2, a family of simulations shows the effect of different values for k_{spin} with a fully-stowed MMS spacecraft performing a $90°$ slew. Immediately evident in the top plot is that, with k_{spin} set to zero, the spacecraft completely fails to maneuver. The bottom plot shows why—no nutation was allowed to develop. The result of nullifying k_{spin} causes the $\hat{\mathbf{s}}$ pointing-term to drop out of of Eq. (30). The inertial target is lost, and the controller acts solely as a nutation damper.

This suggests our parameter-naming may be a slight misnomer. Perhaps "k_{nut}" would be a more descriptive choice. Nevertheless, the k_{spin} label is preserved in this presentation to maintain continuity with its MMS heritage, and the parameter represents the emphasis on orienting the spin-axis inertially.
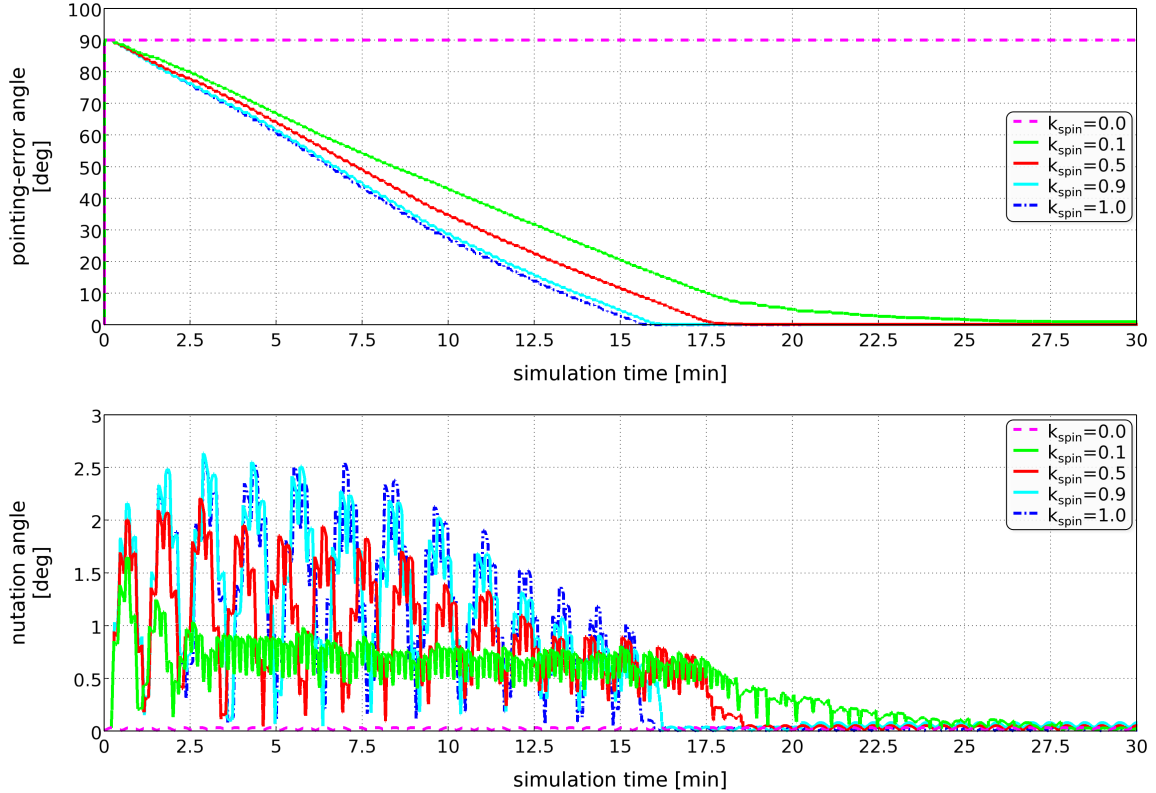

Figure 2. Comparison of $90°$ Slew Performance with Various Values for k_{spin}

On the other end of the spectrum, with k_{spin} set to unity, the control-function is identical to the Reynolds-Creamer method. Figure 2 shows that pointing is aggressively targeted, and the controller has no regard for nutation which builds or cancels intermittently. Slew times are the shortest, but

8

the nutation can increase to unacceptable limits (for MMS) and as will be shown next, the spin-rate can vary significantly.

A value of 0.1 for k_{spin} seems to put a reasonable upper-limit on nutation, and resulted in nearly-linear slew times (convenient for planning)—with asymptotic "clean-up" of both the pointing and nutation errors near the end of a maneuver.

The next pair of plots (Figure 4) is for an even larger slew of $160°$. In this case, the top plot is again pointing-error, but the bottom plot is the spin-rate in revolutions-per-minute. The trivial case of $k_{\mathsf{spin}} = 0$ was also dropped from this set of runs. The surprising result is that for $k_{\mathsf{spin}} = 1$ (i.e. the Reynolds-Creamer control-law), the slew-time is dramatically shorter, but the final spin is now about the *negative* z-axis. The controller has first de-spun the spacecraft—"tunneling" through zero momentum—and then restores spin with the opposite polarity in order to satisfy the momentum-direction-in-inertial-space (i.e. first-term) of the Lyapunov function V_{pw}. When momentum reaches zero, pointing is not defined, so we see a discontinuous jump in the top plot at approximately 4-minutes for both a k_{spin} of 0.9 and 1.

For the remaining values of k_{spin}, the angular rate about the major principal axis dips, but does not become negative. Also note that the spin-rate with k_{spin} of 0.9 does not reach the inverse of the original 3 RPM. This could be an artifact of the modified energy-term that the Reynolds-Creamer and the path weighted formulation share, or a partitioning of the energy due to the partial weighting, but the actual root-cause has not been invested by the authors at the present time since it was not pertinent to MMS.

Figure 3. Angular Momentum Paths on the Celestial Sphere for $160°$ Slew Cases

Without the additional nutation term in the path weighed Lyapunov function, there is nothing to "anchor" the angular-momentum to the body-axes. As a result, for large angles, the system does not slew with the intuitive *great circle* type of motion one might expect. By restricting the angular momentum to remain in the vicinity of a body-fixed vector (in our case the major principal axis, $\hat{\mathbf{p}}_3$), the controller is forced to "drag" the body-axis along with the precession. This notion of great circle paths is the inspiration for the name of the modified control-law, and the weighting in "path weighted" is obviously the free-parameter, k_{spin}. Figure 3 shows the projection of the spacecraft's angular momentum on an inertial-fixed unit sphere for the $160°$ slew cases, and offers an alternative way to visualize the effect the free-parameter has on a body's motion.
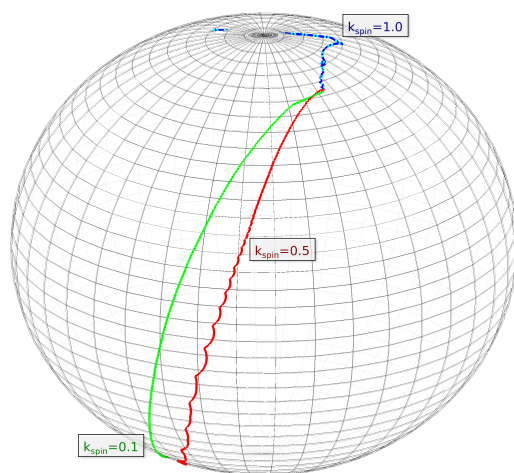
MMS DELTA-H CONTROLLER DESIGN

Moving now from general theory to the specifics of the MMS implementation, Eq. (30) provides a constraint on the polarity of a body-fixed thruster torque $\boldsymbol{\tau}$ that can be checked easily against the Lyapunov constraint through a simple inner-product multiplication with the vector in brackets—the resulting scalar must be negative for a given combination of thrusters to be a candidate for actuation. However, there are a few additional considerations made in the MMS design that elevates a possible candidate first to an "eligible", and then a "best" candidate. The next three subsections explore some
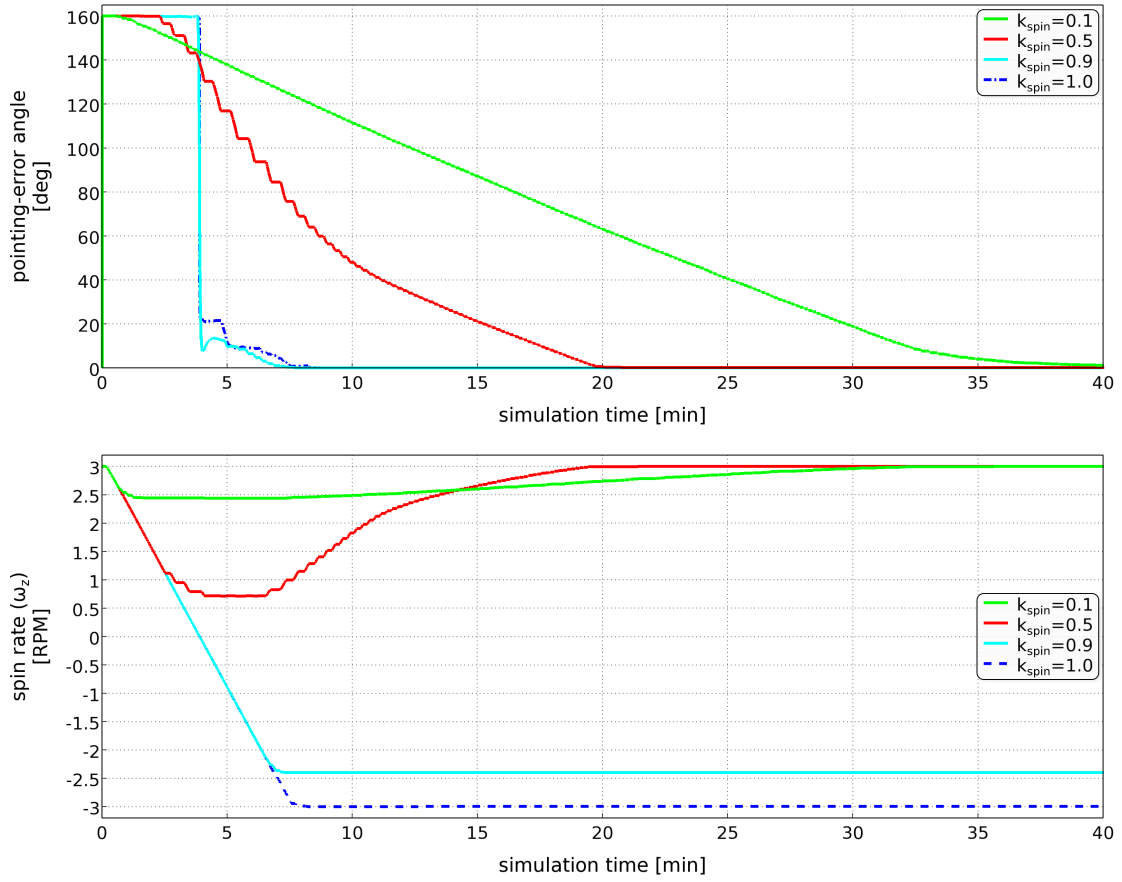
Figure 4. Comparison of 160° Rigid-Body Slew Performance with Various Path Weights

these additional criteria with regard to efficiency, deadbands, and bandwidth. They are followed by the topic of multi-body dynamics and associated stability. Finally, flight performance is compared to simulation predictions for MMS's largest fully-deployed slew, and then a collection of smaller maintenance maneuvers.

Efficiency

Propellant efficiency is a primary consideration for any mission. While it would make sense to only fire a thruster when its torque-axis is aligned as close to 180° away from the rate-error as possible, this is not always practical. Instead, the inner-product resultant is checked not only for its sign, but also its normalized magnitude. If the normalized magnitude is greater than the cosine of an efficiency angle ε, then the torque is considered sufficiently well aligned. This logic is analogous to Reynolds and Creamer's presentation

`if`
$$\cos\varepsilon < \frac{[-\boldsymbol{\delta\omega}_{\mathsf{pw}}]^{\mathsf{T}}\,\boldsymbol{\tau}}{\|\boldsymbol{\delta\omega}_{\mathsf{pw}}\|\,\|\boldsymbol{\tau}\|} = \frac{[-\boldsymbol{\delta\omega}_{\mathsf{pw}}]^{\mathsf{T}}\,\hat{\boldsymbol{a}}_{\boldsymbol{\tau}}}{\|\boldsymbol{\delta\omega}_{\mathsf{pw}}\|} \tag{33}$$
`then`
`   OK to fire thruster-bank`

10

where $\hat{\mathbf{a}}_\tau$ is a unit vector along the torque axis. In a given control-cycle, MMS extends this check to all moment-couples of thrusters, called "banks", and tags the most efficient pair as candidates to fire at the next opportunity. Before actually issuing the thruster commands, the controller makes a few additional checks against both deadbands, and wait-counters as discussed below.

Making the cosine-efficiency-angle ε small reduces fuel-waste, but can also introduces issues of coverage. MMS, like many spinners, relies on the natural motion of the angular rate in the body-frame to bring the rate-error into alignment with a limited set of spin-plane thrusters. With too small of an efficiency angle, it's possible to introduce dead-zones that the badly-aligned angular rate-error travels without ever triggering actuation.

This situation is shown pictorially in Figure 5 for an efficiency angle of $16°$. The rate-error (blue) must intersect one of the red *small circles* in order to satisfy Eq. (33). Fortunately, multi-body dynamics tend to disrupt the stability of some unfavorable rate-error trajectories, and can actually improve the effective coverage. MMS used this knowledge to reduce its cosine-efficiency criteria shortly after its perigee raise maneuvers—its last in the fully-stowed configuration.
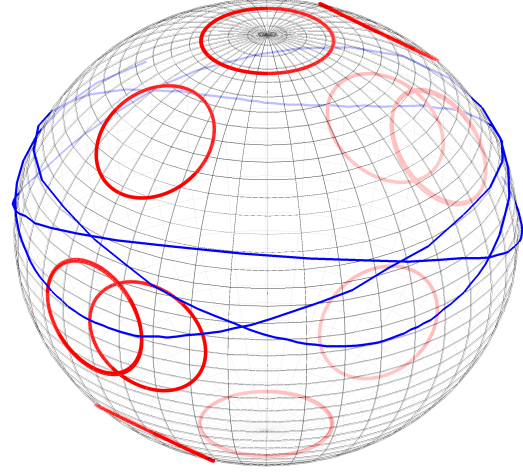

Figure 5. Control Coverage on Body Sphere

Deadbands

As the controller nears its target, deadbands are effective tools for combating *chatter* (unproductive and excessive control that attempts to correct for noise or overshooting). For MMS a deadband was achieved by limiting the size of the minimum pulse-duration for thruster commands. The MMS thrusters (in conjunction with a GSFC designed valve-driver) was capable of executing pulses as short as 20 msec—although in practice 50 msec was found to be a more effective lower limit. The required size of a pulse is determined on-board at each control-cycle using a scalar approximation of *Euler's rotational equation* ($\tau = I\Delta\omega/\Delta t$), with the spacecraft's second mass-moment of inertia $\mathbf{I}$ and rate error $\boldsymbol{\delta\omega}_{\mathsf{pw}}$ projected along the thruster-bank's torque-axis $\hat{\mathbf{a}}_\tau$ so that

$$\Delta t_{\mathsf{pulse}} = \frac{\hat{\mathbf{a}}_\tau^\mathsf{T}\,\mathbf{I}\,\hat{\mathbf{a}}_\tau}{\|\boldsymbol{\tau}\|} \cdot [-\boldsymbol{\delta\omega}_{\mathsf{pw}}]^\mathsf{T}\,\hat{\mathbf{a}}_\tau \tag{34}$$

The calculated pulse-duration $\Delta t_{\mathsf{pulse}}$ is also limited to be slightly shorter than a control-cycle. When the SDP are deployed, the physical moment of inertia $\mathbf{I}$ is replaced with an "effective" inertia as described in Zimbelman and Walker.[8] The effective moment of inertia about the spin-axis is

$$I_{\mathsf{eff}} \equiv I_{\mathsf{base}} + \left(\frac{r_{\mathsf{sdp}}}{r_{\mathsf{sdp}} + L_{\mathsf{sdp}}}\right) I_{\mathsf{sdp}} \tag{35}$$

where r_{sdp} is the radial distance from the spin-axis to the SDP pivot-point, L_{sdp} is the distance along the wire boom to the SDP's center-of-mass, and I_{sdp} is the SDP's second mass-moment of inertia about its own center-of-mass, as if it were a rigid rod. A similar expression is also used for the effective inertias about the spacecraft's transverse axes.

Mode Auto-exit

MMS incorporated another feature in its controller design that was also intended to conserve propellant at the end of a maneuver. The magnitude of the rate-error $\delta\omega_{pw}$ was fed through a digital low-pass filter tuned to the behavior of our system. The system's deadband was subtracted from the filtered result, and the remainder compared against the auto-exit criteria. In order to protect against over-shoot in this filter, a minimum and maximum time-in-mode requirement is enforced, and a hysteresis count-down timer is also applied. Figure 6 shows the filtered/rectified rate-error for the $90°$ slew cases.
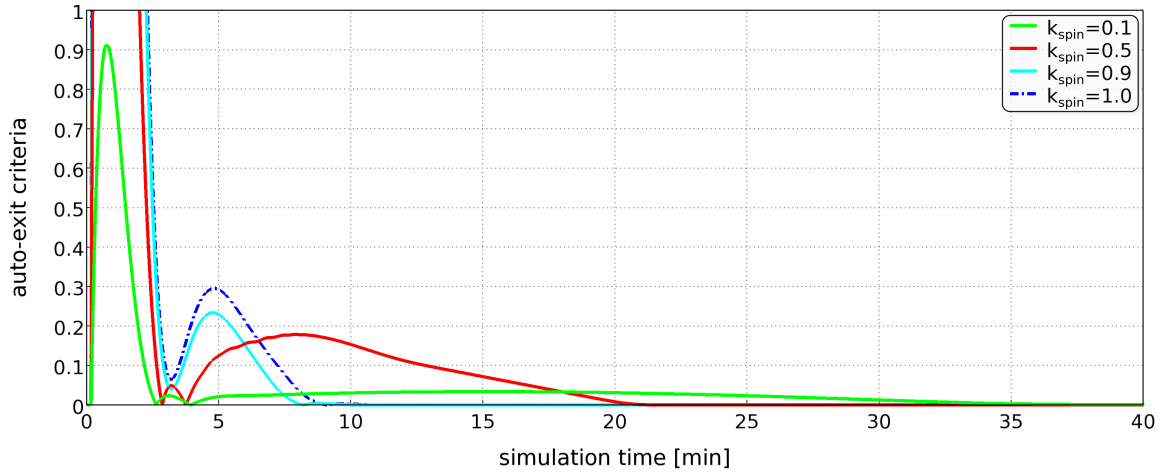
Figure 6. Auto-exit Criteria for $90°$ Slew Cases

Bandwidth

Skipping control-cycles via a digital wait-counter effectively reduces the bandwidth of the controller. Like deadbands, this can help to reduce chatter caused by fighting the high-frequency noise in the rate estimate. MMS adjusted its wait-counter settings depending on its boom deployment state. In the section that follows, the effect of delays on low-frequency flexible body dynamics will be discussed.

Appendage Multi-body Dynamics

Up until now, all of the discussion and examples have focused on the behavior of a spacecraft that is well approximated by a rigid-body. However, when fully-deployed, the SDP wire booms span a total of 120-meters in diameter and are far from rigid. While Lyapunov-control based on a function that uses total mechanical energy is known to be very robust to the presence of modeling error[5] (e.g. inertia tensor), the SDP degrees of freedom do not explicitly appear in the work-energy relationship that was used for the path weighted formulation. As a result, it remained an open-issue during the MMS design phase if the Lyapunov stability guarantees would still apply. While a number of analytic models for the system were used to provide insight on the system's modes,[9,3,10] a multi-body Lyapunov function was never attempted. As the system analysts, the authors chose to instead rely on Monte Carlo methods applied to time-domain simulations in order to verify both stability and performance of the non-linear system using the path weighted controller.

In the course of our investigations, it became evident that it was possible to slew the fully-deployed spacecraft over an arbitrarily large path given a sufficient maneuver window. Inspired by the way the *gravity gradient* environmental torque could slowly precess the angular momentum of the spacecraft without exciting the SDP booms, we determined the key ingredients of a successful strategy were: small thrusts and proper delays.
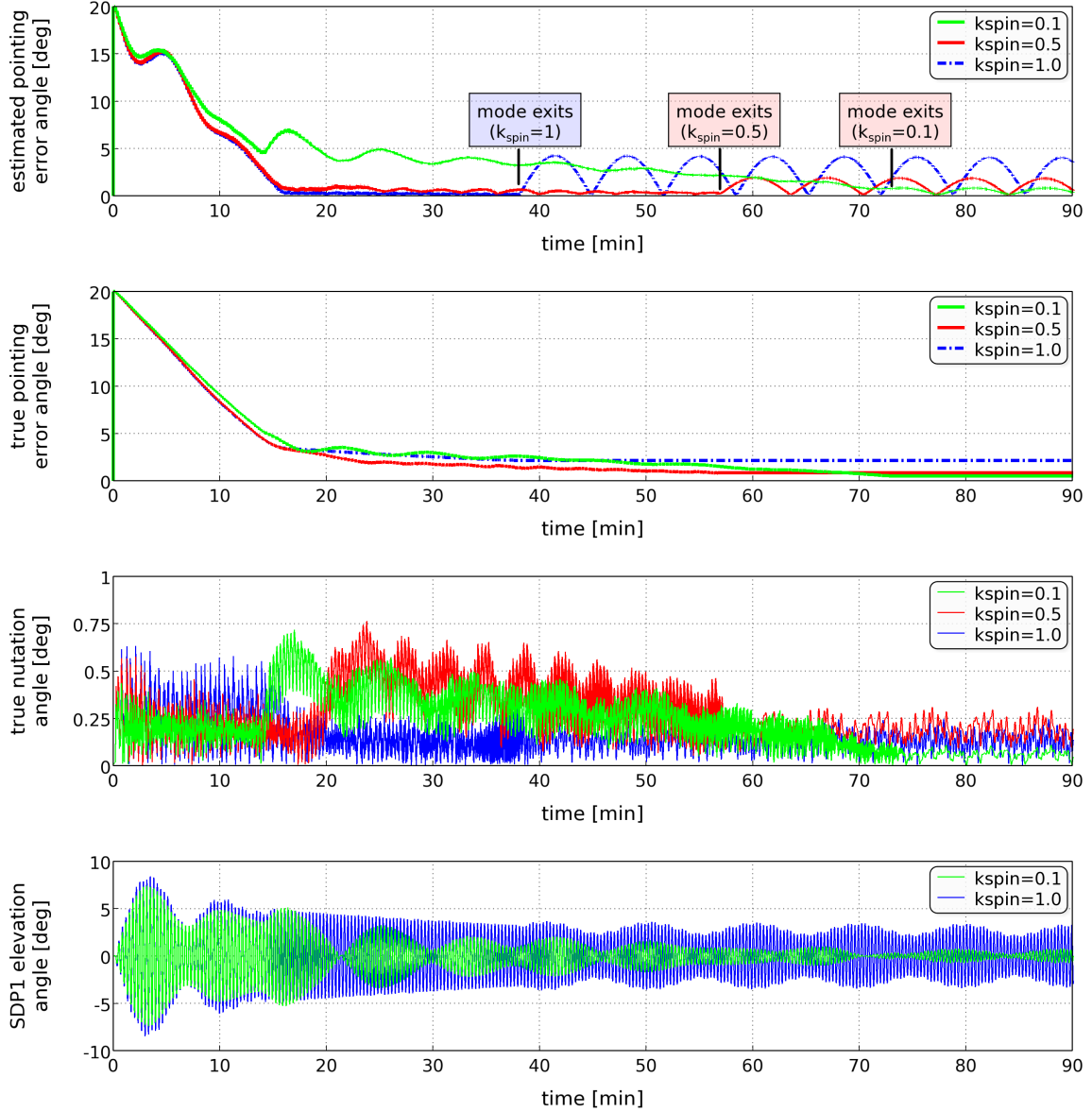

Figure 7. Comparison of $20°$ Multi-Body Slew Performance with Various Path Weights

Figure 7 shows a $20°$ slew for various values of the path-weighting variable k_{spin}. What is interesting to note is that for larger weights, the total system momentum (base-body + appendages) fails to finish close to the target. Specifically, with a k_{spin} of 1, the final pointing error is about $2.1°$. This is due to the unobservable momentum of the SDP booms. The more aggressive slew, essentially moves (and briefly holds) the base-body at the desired inertial attitude, leaving the booms behind. After the auto-exit counter has timed out (around 38-minutes), the SDPs drag the base-body back

to an attitude closer to the true system momentum. In contrast, the more gentle path ($k_{\text{spin}} = 0.1$) has a final true pointing error of less than $0.5°$, but takes over 73-minutes to satisfy the exit criteria.

The characteristic humps after mode-exit of the top plot in Figure 7, is the rectified coning of the base-body. Its presence in the telemetered pointing-estimate is a good indication of the magnitude of the SDP boom excitation that occurred during a maneuver (see also Figure 9).

Monte Carlo Performance Results

As part of the design process, Monte Carlo methods are used to access robustness of the controller, both in terms of performance with plant-uncertainties and overall stability. For MMS, exhaustive Monte Carlo simulations were used to address these twin concerns. Following the statistical methodology of Hanson and Beard,[11] a 99% confidence criteria (1% consumer risk) was selected that requires zero failures over a sample-size of 3410 runs.

This criteria was tested repeatedly using GSFC's *Freespace Simulation Environment*[12] to statistically vary over 250 model parameters—resulting in hundreds of thousands of time-domain simulations of maneuvers at full model-fidelity. Figure 8 depicts one example of these results, and is annotated with the performance criteria used to determine execution error acceptance for a formation-maintenance class of Delta-H slews (i.e. $1.3°$ over 20-minutes to less than $0.2°$) that are performed with the fully-deployed observatory immediately after a translational orbit-adjustment ranging in size from 0–10 m/sec and capable of exciting up to $2.5°$ (amplitude) of wire boom oscillation (3σ). In the figure, the "post ΔV" angle (in blue) is the orbit-adjustment's perturbation on the initial pointing, so it will add (or subtract) to the total slew-size required of the Delta-H mode.
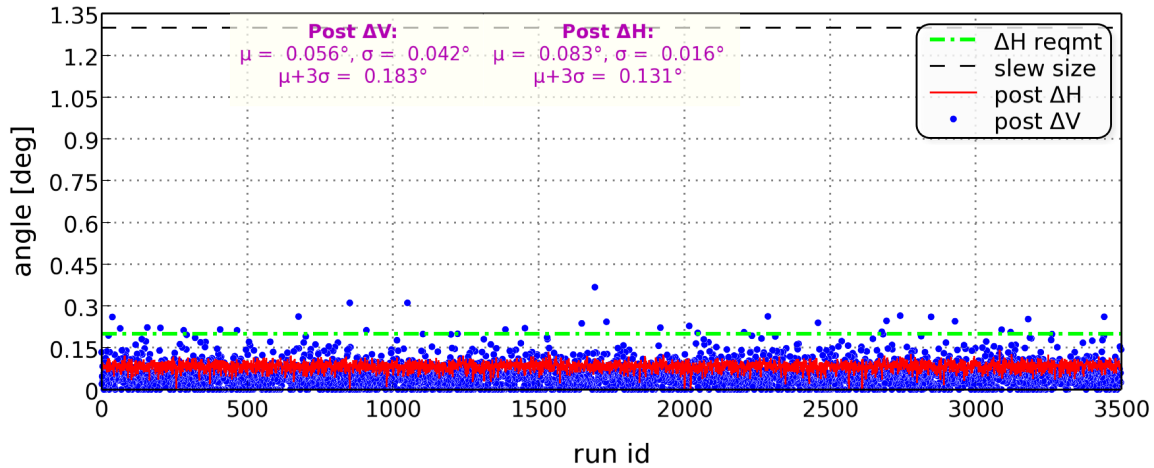

Figure 8. Monte Carlo Results for 3500 samples of a Formation Maintenance Class of Slews

MMS Mission Performance

In this section, some flight performance results of the MMS Delta-H Mode are shown for a $17°$ slew made by MMS-3 on July 8, 2015 (HA088) in the fully-deployed configuration. The plots in Figure 9 show (in red) the telemetered flight-data along with the simulation predictions used to plan the maneuver (in blue). In this instance, the simulation conservatively predicts more nutation than the on-board flight-estimate shows, and is slightly faster at reaching the target. The difference is within the expected bounds. The peak SDP out-of-plane (elevation) amplitude for this maneuver was—from simulation—less than $1.74°$, and in-plane (azimuth) peaked at only $0.14°$. To some
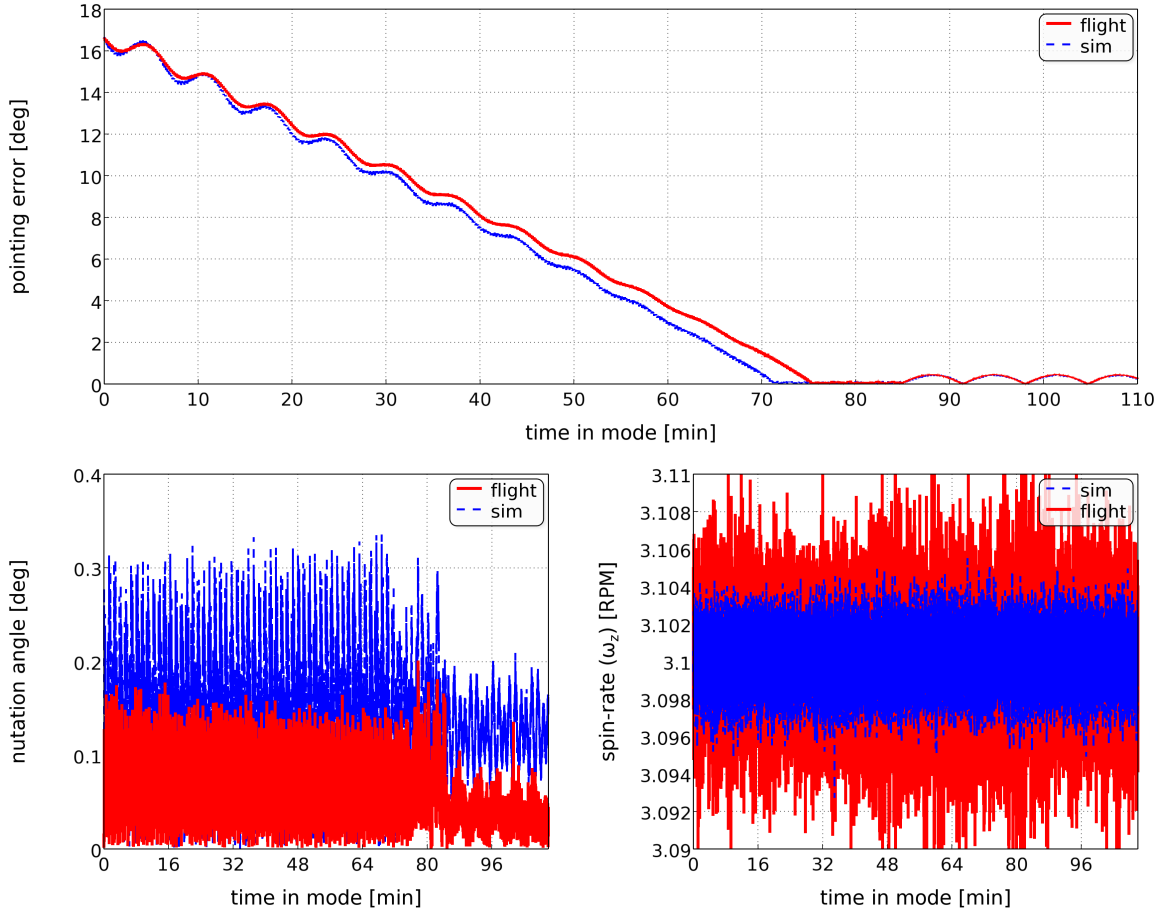
Figure 9. Flight Performance of an MMS-1 10° Slew Compared to Simulation ($k_{\mathsf{spin}} = 0.1$)

extent, the SDP excitation-levels were confirmed by the science-instrument's telemetry, which can detect displacements great than $5°$. As predicted by simulation, no oscillations were detected. Also, the size of the pointing-error "humps" in the flight telemetry after mode-exit (at 85-minutes) attests to a well-managed amount of SDP motion for the mission's largest fully-deployed slew.

As MMS nears the completion of its commissioning phase, the size and frequency of the maneuvers have become both smaller and more regular. The main driver for maintenance slews is to keep the spin-axis canted 2.36–$3.80°$ towards the sun for the remainder of the mission. Given a 40-minute total maneuvering window, the Delta-H mode is required to precess the fully-deployed spacecraft's angular momentum by up to $2.6°$ an average frequency of less than once every two weeks using a single (or equal pair of) maneuvers whose final pointing accuracy is $0.2°$ (3σ).

The table in Figure 10 shows the twelve most recent flight maneuvers that utilized Delta-H mode. For the subset of slews that were allocated 20-minutes to complete, the sample mean $\bar{\mu}$ of the final pointing error is $0.131°$, and the sample standard deviation $\bar{\sigma}$ is $0.068°$. This targeting accuracy plays a role in preventing loss of shadowing on some of the boom's tip-sensors due to both solar precession of the orbit ($\approx 1°$/day), and gravity-gradient pointing disturbances over a two-week period. The statistics will continued to be monitored closely as the mission progresses. A number of command-able control parameters are available to tune the system further, if necessary.

15

Maneuver (DOY)	Observatory ID	Maneuver Duration (min)	Magnitude of Slew (degrees)	Final Pointing Error Estimate (degrees)
GS-095 (167,168)	1	40	2.49	0.24
	2	40	2.66	0.29
	3	20	0.87	0.25
	4	40	2.39	0.15
DH-116	1	40	2.18	0.06
FI-116 (188)	2	20	1.43	0.06
	3	20	1.07	0.16
	4	20	1.18	0.11
FI-119 (190)	1	—	—	—
	2	20	1.31	0.05
	3	20	1.21	0.15
	4	20	1.21	0.14

Figure 10. Formation Maintenance Maneuver Statistics

CONCLUSION

A new Lyapunov-based control-law has been presented that extends the work of Reynolds and Creamer.[4] It provides a complete solution to the coupled dynamics problems of precession, nutation, and spin-rate control of a spinning spacecraft. Through a single free-parameter, a controls engineer may adjust the nature of a slew-path—choosing between aggressive targeting, or benign trajectories that preserve spin-stability.

Rigorous ground testing and on-orbit experience from the MMS mission have shown that the derived controller is both robust and intuitively simple to use, even for a spacecraft with complex appendage dynamics.

ACKNOWLEDGMENTS

REFERENCES

[1] F. Markley and J. L. Crassidis, *Fundamentals of Spacecraft Attitude Determination and Control*. Space Technology Library, Springer, 1st ed., 2014.

[2] J. K. Thienel, F. L. Markley, and R. R. Harman, "Extended Kalman Filter for MMS State Estimation," *Advances in Astronautical Science*, AAS/AIAA Space Flight Mechanics Meeting, 2009, pp. 1513–1526. AAS 09-202.

[3] T. G. McGee, U. J. Shankar, and B. L. Kemp, "Analysis of Spinning Spacecraft with Wire Booms, Part 2: Out-of-Plane Dynamics and Maneuvers," *AIAA Guidance, Navigation and Control Conference*, No. 2009-6203, August 2009.

[4] R. Reynolds and G. Creamer, "Global Lyapunov Control of Spin Stabilized Spacecraft," *2001 Flight Mechanics Symposium* (J. P. Lynch, ed.), No. NASA/CP–2001-209986, NASA Goddard Space Flight Center, Greenbelt, MD, June 2001, pp. 285–294.

[5] H. Schaub and J. L. Junkins, *Analytical Mechanics of Space Systems*. American Institute of Aeronautics and Astronautics, Inc., 1st ed., 2003.

[6] B. Wie, *Space Vehicle Dynamics and Control*. AIAA Inc, Reston, VA: American Institute of Aeronautics and Astronautics, Inc., 2nd ed., 2008.

[7] B. Wie and P. Barba, "Quaternion Feedback for Spacecraft Large Angle Maneuvers," *Journal of Guidance, Control, and Dynamics*, Vol. 8, No. 3, 1985, pp. 360–365.

[8] D. Zimbelman and M. Walker, "FAST AURORAL SNAPSHOT Performance Using a Multi-Body Dynamic Simulation," *Advances in Astronautical Science*, AAS Spaceflight Dynamics, 1993. AAS 93-334.

[9] S. Lai and K. Bhavnani, "Dynamics of Satellite Wire Boom Systems," Tech. Rep. AFCRL-TR-75-0220, Air Force Cambridge Research Laboratories, Torrance, CA, February 1975.

[10] S. Queen, K. London, and M. Gonzalez, "Momentum-Based Dynamics for Spacecraft with Chained Revolute Appendages," *Flight Mechanics Symposium*, NASA Goddard Space Flight Center, Greenbelt, MD, Oct 2005.

[11] J. M. Hanson and B. B. Beard, "Applying Monte Carlo Simulation to Launch Vehicle Design and Requirements Verification," *AIAA Guidance, Navigation and Control Conference*, Ontario, Canada, August 2010. AIAA 2010-8433.

[12] P. M. Hughes, "NASA Goddard Space Flight Center FY 2006 Internal Research and Development Program," Tech. Rep. 2006-AR-V6, NASA/Goddard Space Flight Center, Greenbelt, MD, 2007.